A&A 553, A83 (2013)
DOI: 10.1051/0004-6361/201321056

Astronomy & Astrophysics

A bright thermonuclear X-ray burst simultaneously observed with *Chandra* and RXTE

J. J. M. in 't Zand[1], D. K. Galloway[2], H. L. Marshall[3], D. R. Ballantyne[4], P. G. Jonker[1,5,6], F. B. S. Paerels[7], D. M. Palmer[8], A. Patruno[9], and N. N. Weinberg[3]

[1] SRON Netherlands Institute for Space Research, Sorbonnelaan 2, 3584 CA Utrecht, The Netherlands
e-mail: `jeanz@sron.nl`
[2] Monash Centre for Astrophysics, School of Mathematical Sciences & School of Physics, VIC 3800, Monash University, Australia
[3] Dept. Physics and Kavli Institute for Astrophysics and Space Research, Massachusetts Institute of Technology, Cambridge, MA 02139, USA
[4] Center for Relativistic Astrophysics, School of Physics, Georgia Institute of Technology, Atlanta, GA 30332, USA
[5] Harvard-Smithsonian Center for Astrophysics, 60 Garden Street, Cambridge, MA 02138, USA
[6] Department of Astrophysics/IMAPP, Radboud University Nijmegen, PO Box 9010, 6500 GL Nijmegen, The Netherlands
[7] Columbia Astrophysics Laboratory, 550 West 120th Street, New York, NY 10027, USA
[8] Los Alamos National Laboratory, B244, Los Alamos, NM 87545, USA
[9] Astronomical Institute "Anton Pannekoek", University of Amsterdam, Science Park 904, 1098 XH Amsterdam, The Netherlands

Received 8 January 2013 / Accepted 19 March 2013

ABSTRACT

The prototypical accretion-powered millisecond pulsar SAX J1808.4−3658 was observed simultaneously with *Chandra*-LETGS and RXTE-PCA near the peak of a transient outburst in November 2011. A single thermonuclear (type-I) burst was detected, the brightest yet observed by *Chandra* from any source, and the second-brightest observed by RXTE. We found no evidence for discrete spectral features during the burst; absorption edges have been predicted to be present in such bursts, but may require a greater degree of photospheric expansion than the rather moderate expansion seen in this event (a factor of a few). These observations provide a unique data set to study an X-ray burst over a broad bandpass and at high spectral resolution ($\lambda/\Delta\lambda$ = 200–400). We find a significant excess of photons at high and low energies compared to the standard black body spectrum. This excess is well described by a 20-fold increase of the persistent flux during the burst. We speculate that this results from burst photons being scattered in the accretion disk corona. These and other recent observations of X-ray bursts point out the need for detailed theoretical modeling of the radiative and hydrodynamical interaction between thermonuclear X-ray bursts and accretion disks.

Key words. accretion, accretion disks – X-rays: binaries – X-rays: bursts – stars: neutron – X-rays: individuals: SAX J1808.4-3658

1. Introduction

The vast majority of thermonuclear X-ray bursts from neutron stars (the so-called type I X-ray bursts, see e.g., Lewin et al. 1993; Strohmayer & Bildsten 2006) have been measured with instruments that are sensitive at photon energies above 2 keV. The temperature of type-I X-ray bursts is, however, 2.5 keV or lower so that usually a substantial part of the spectrum is missed. Therefore, interesting physics may be missed, particularly during the cooler parts of X-ray bursts in the tail and during phases of photospheric expansion. Not only that: many of the discrete atomic spectral features from abundant elements in the cosmos (oxygen, neon and iron) occur below 2 keV. Sub-2 keV measurements of X-ray bursts at high spectral resolution and with photospheric expansion are, therefore, interesting to pursue.

Since the launch of *Chandra* and *XMM-Newton* in 1999 and *Swift* in 2004, sub 2 keV coverage is readily available. However, these are narrow field instruments where measurements are usually made through a dedicated program, in contrast to the wide-field instruments on board SAS-B, *BeppoSAX*, INTEGRAL, *Swift* and *Fermi* that lack sub 2 keV coverage. We estimate that about 250 X-ray bursts have been detected below 2 keV with these three missions, compared to about 10^4 with the wide field instruments (e.g., Cottam et al. 2002; Jonker et al. 2003; Thompson et al. 2005; Boirin et al. 2007; Kong et al. 2007; Paizis et al. 2012). Hardly any X-ray bursts with photospheric expansion and low $N_{\rm H}$ were detected with sub 2 keV coverage so far, perhaps 6 with low flux (Galloway et al. 2010).

In this paper we report an observation of a bright thermonuclear burst with photospheric expansion from the low-mass X-ray binary (LMXB) SAX J1808.4−3658, with the AXAF CCD Imaging Spectrometer (ACIS) in combination with the Low-Energy Transmission Grating Spectrometer (LETGS) on board *Chandra*. The event was detected simultaneously with the RXTE Proportional Counter Array (PCA). Combined this presents a unique data set with, as far as we know, the largest number of photons ever detected from a single X-ray burst in the 0.5–2 keV band or with a grating spectrometer.

SAX J1808.4−3658 is the first discovered accretion-powered millisecond X-ray pulsar in a LMXB (in 't Zand et al. 1998; Wijnands & van der Klis 1998; in 't Zand et al. 2001; Chakrabarty et al. 2003), of 14 cases known thus far (e.g., Patruno & Watts 2012). It is also a relatively nearby representative, at 3.5 ± 0.1 kpc (Galloway & Cumming 2006), and with a relatively low column density of interstellar material ($N_{\rm H}$ = (1–2) × 10^{21} cm^{-2}; e.g., Wang et al. 2001; Papitto et al. 2009; Cackett et al. 2009). Almost all its X-ray bursts exhibit photospheric expansion (Galloway et al. 2008) and the bursts appear to be the result of a flash of a pure helium layer that is produced by stable hydrogen burning. These circumstances make SAX J1808.4−3658 a particularly suitable source to study X-ray bursts in great detail and in a large bandpass. Therefore, we observed SAX J1808.4−3658 with *Chandra* and RXTE during its November 2011 outburst.

The main goal of our measurement was to search for absorption edges. We were motivated by a prediction of Weinberg et al. (2006) that the radiative wind of radius expansion bursts eject ashes of nuclear burning whose spectral signature may be detectable with current high-resolution X-ray telescopes. This may be the best path to finding discrete spectral features from neutron star (NS) surfaces, whose detection could constrain thermonuclear reactions in the NS ocean and the NS compactness through general relativistic gravitational redshift determinations. Near-Eddington X-ray bursts reveal themselves as having black body like spectra with phases of expanded emission areas. There are two kinds: those with moderate expansion (factor ~10 increase in emission area), encompassing ≈20% of all bursts, and those with superexpansion (factor $\gtrsim 10^4$), encompassing perhaps ~0.1% of all bursts (e.g., van Paradijs et al. 1990; Galloway et al. 2008; in 't Zand & Weinberg 2010). The difference in expansion is likely determined by whether an optically thick shell is being expelled which on its turn is determined by how much the radiative flux from the nuclear burning goes over the Eddington limit in the flash layer. Also, the larger this super-Eddington factor is, the larger the upward extent of the convection and the probability for absorption edges will be. The burst we discuss here is a bright burst from a relatively nearby NS and, ergo, of good statistical quality. However, it has only a moderate photospheric expansion.

We introduce the observations in Sect. 2, including monitoring observations with the Monitoring All-sky X-ray Imager (MAXI) on board the International Space Station (ISS) and the Burst Alert Telescope (BAT) on board *Swift*, and provide the details of the data reduction in Sect. 3. Section 4 discusses the spectral analysis and Sect. 5 briefly the timing behavior of the detected burst. Finally, in Sect. 6, we place the results in the context of the theory of burst spectra.

2. Observations

On November 4, 2011, a new outburst of SAX J1808.4−3658 was reported from *Swift*-BAT observations beginning October 31 (Markwardt et al. 2011). Figure 1 shows the outburst light curves from MAXI, RXTE-PCA and *Swift*-BAT data. MAXI (Matsuoka et al. 2009) is deployed on the International Space Station (ISS) and, in combination with the Gas Scintillator Counter (GSC), is active between 2 and 30 keV. The measurements consist of 1 min exposures every 100-min ISS orbit and are made public within a few hours of being taken[1]. BAT (Barthelmy et al. 2005) is a gamma-ray burst monitor camera active on *Swift* between 15 and 100 keV. The 15–50 keV flux of some 500 X-ray sources are monitored several times per day and made available publicly in near real time[2]. The PCA data (see below) were obtained under ObsID 96027-01 for a total exposure time of 143.6 ks (see also Patruno et al. 2012, and below).

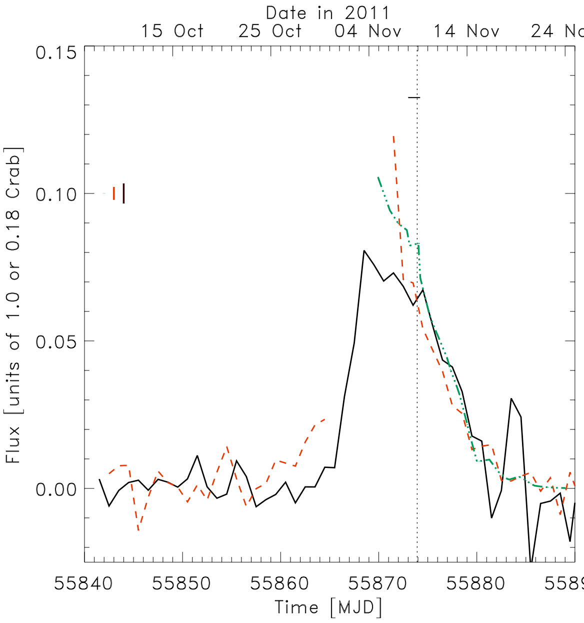

Fig. 1. Light curves of the 2011 outburst of SAX J1808.4−3658: from 2–10 keV RXTE/PCA data (green dash-dotted line, normalized to 1580.5 c s^{-1} PCU^{-1} equivalent to 1.0 Crab unit; see also Patruno et al. 2012), 2–10 keV MAXI/GSC data (red dashed line; normalized to 3.2 c s^{-1} cm^{-2} equivalent to 1.0 Crab unit) and 15–50 keV *Swift*/BAT data (black solid line; normalized to 0.22 c s^{-1} cm^{-2} equivalent to 0.18 Crab units). The outburst started on MJD 55 865 (Oct. 31st) and lasted for 21 d, until MJD 55886. The horizontal solid line indicates the time frame of the *Chandra* observation and the vertical dotted line through it the burst that was detected with *Chandra* and RXTE. The vertical bars at mid left indicate the typical 1σ uncertainty per data set (PCA flux errors are typically smaller than the line thickness). (Color version of figure available in online version.)

Following the alert, we requested and were granted a *Chandra* target of opportunity observation (ObsID 13718). The exposure time is 100.13 ks between Nov. 8 00:46 UT and Nov. 9 04:35 UT (see Fig. 2) which is 8 days after the presumed outburst onset. The observatory was operated using the Low-Energy Transmission Grating Spectrometer (LETGS; Brinkman et al. 2000), with ACIS-S (Garmire et al. 2003) at the focal plane and the Low-Energy Transmission Grating in the beam. This combination provides a marginally higher effective area than the HETGS (see e.g., proposers' observatory guide Fig. 1.4) in most of the interesting bandpass of 0.5–6 keV at the expense of some spectral resolution. The resolution is, however, sufficient to search for absorption edges ($\lambda/\Delta\lambda$ = 200–400). A disadvantage of using ACIS instead of HRC is the loss of effective area between 0.08 and 0.5 keV, but this bandpass is of no interest to this observation because the source is significantly absorbed there. To avoid pile up, ACIS was operated in the continuous clocking (CC) mode. In this mode, position information is lost in the cross dispersion direction while the time resolution is improved from 3.2 s to 2.85 ms. The disadvantage is that the background cannot accurately be measured independently (it is possible to discriminate with some sensitivity the background from source in pulse height versus dispersion space), but this is not detrimental because we are primarily interested in X-ray bursts which can easily be separated in the time domain, without the need for the spatial resolution. Four ACIS CCDs were employed: S1 through S4. The offset of the Science Instrument Module (the

---

[1] `http://maxi.riken.jp/top`

[2] `http://swift.gsfc.nasa.gov/docs/swift/results/transients`

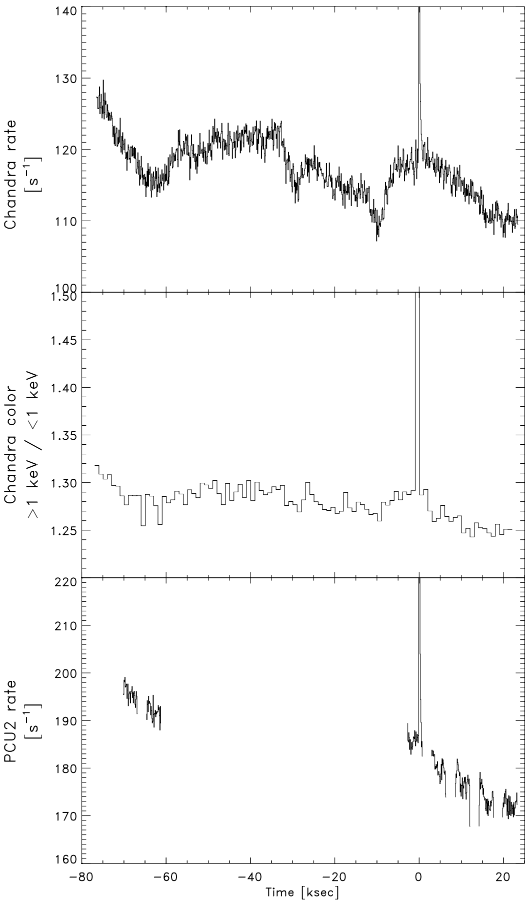

Fig. 2. Time histories of total *Chandra*-observed photon rate, measured over all active ACIS-S CCDs, at 100 s resolution (*top panel*), the color at 1000 s resolution (*middle panel*) and the RXTE PCU2 rate at 100 s resolution (*bottom panel*). The burst peak has been cut in all panels. No background was subtracted.

so called "SIM offset") was –8 mm to position the dispersed spectrum as close as possible to the CCD edges to optimize the CCD spectral resolution. The Y offset was +1.6 arcmin so that the zeroth order would be detected by S2.

Simultaneous measurements were requested and granted with RXTE under proposal number 96027. Twenty-four ks of simultaneous coverage was obtained (see Fig. 2). The Proportional Counter Array (PCA; Jahoda et al. 2006) comprises 5 non-imaging proportional counter units (PCUs) active between 2 and 60 keV with a combined effective area of 6000 cm^2 at 6 keV. The spectral resolution is 18% full width at half maximum at 6 keV and the time resolution of the data products for SAX J1808.4–3658 is typically 125 μs. It is seldom that all PCUs are active at the same time, particularly at late times in the mission. During our observations, PCA operated with 2 active proportional counter units (PCUs 1 and 2, counted from 0). All PCUs have collimators delimiting the field of view to $2^\circ \times 2^\circ$ (full width to zero response). For our analysis, we used standard-1 and 2 data (time resolution 0.125 and 16 s, energy resolution 1 and 128 channels, respectively) and event mode data `E_125us_64M_0_1s` with 125 μs time resolution and 64 energy channels between 2 and 60 keV. All data allow selection of PCUs.

Figure 2 shows the *Chandra* and PCA-measured (only PCU2) light curves during the time of the *Chandra* observation. These curves show the detection of one burst in both instruments. This is the only X-ray burst detected from SAX J1808.4–3658 in the whole outburst (cf., Patruno et al. 2012). RXTE and *Chandra* times were synchronized by matching the burst onset as seen in the overlapping bandpass 3–8 keV. We find that the burst starts at MJD 55 873.91320 (barycentered), or at RXTE time[3] 563 407 175.90 s and *Chandra* time[4] 437 176 836.46 s (not barycentered). There is simultaneous *Chandra*/RXTE coverage between –2560 and +812 s with respect to the burst onset time (see Fig. 3). The total number of burst photons detected is 38 800 ± 180 with *Chandra* (measured over the complete ACIS-S detector and after subtraction of a pre-burst level) and 562 800 ± 400 with RXTE. The peak intensities, measured at 0.125 s time resolution, are 2538 c s^{-1} for *Chandra* (all ACIS events, not corrected for non-burst events) and 33 669 c s^{-1} for RXTE. The *Chandra* net peak rate for orders –1/+1 is 1930 c s^{-1}. The *Chandra* event data buffer of 128 000 events (in the graded telemetry mode) was not overfilled. The RXTE data buffer was overfilled. Starting at 1.15 s after burst onset, 0.45 s chunks of data are missing in the event-mode data every 1.0 s until 10.6 s. After that 3 smaller chunks of 0.45 s are missing every 1.0 s until 13.6 s after which the data are completely recovered. The standard-1 and 2 data do not have gaps.

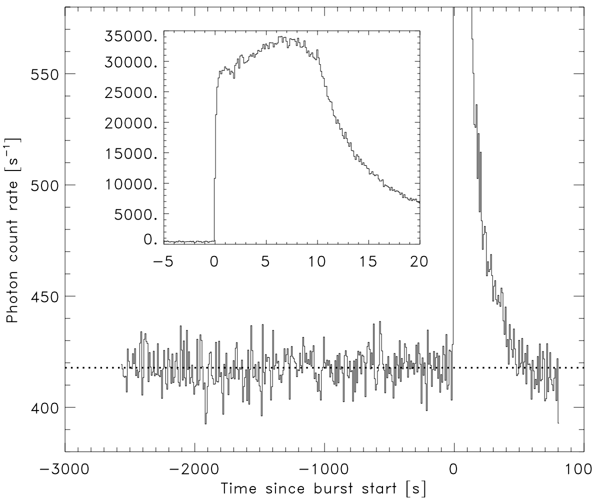

Fig. 3. Time history of RXTE detected photon rate around the burst, at 8 s resolution. Photons detected with PCUs 1 and 2 have been combined. The dotted horizontal line shows the fit with a constant line to the data prior to the burst (with a best-fit value of 418 s^{-1}). The burst lasts 550 ± 20 s. The inset zooms in on a 25 s stretch around the peak, at 1/8 s resolution.

The non-burst emission varied significantly during the 100 ks of the *Chandra* observation. The intensity decreased from 128 to 110 c s^{-1}, or 14% although this is not corrected for the background (which is expected to be a few c s^{-1}). The decrease is not smooth. The *Chandra* color history, the color being defined as the intensity of all ACIS events above 1 keV divided by that below, also shows a gradual decrease by 5%.

3. Data reduction

There are 11.79 million events in the *Chandra* event file, equivalent to an average count rate of 117 c s^{-1}, in 4 ACIS-S detectors. The 0th order contains 3.56 million events (30%), –1/+1 orders

---

[3] Mission elapsed time, defined as seconds since 1994.0 UTC.

[4] Mission elapsed time, defined as seconds since 1998.0 TT.

contain 2.43/3.29 million events, orders –2/+2 0.12/0.14 million events, orders –3/+3 0.27/0.28 million events. We investigated only orders –1 and +1 since these encompassed 7.1 times more photons than orders –2/+2 and –3/+3 combined.

We reduced the *Chandra* data with `ciao` version 4.4, `ftools` version 6.12 and CALDB version 4.5.0. `tgextract` was used to extract the grating order data from the event-2 file, after the eventfile was filtered for a particular time interval with `dmcopy`, including a workaround[5] for a bug in `ciao` versions 4.3 and 4.4 concerning incorrect GTIs when time-filtering grating data with `dmcopy`. The resulting pha2 file was divided into separate orders with `dmtype2split`. `fullgarf` was used to obtain ancillary files for each time interval separately, `mkgrmf` for the response files (only one file for all time intervals). We excluded data around three absorption edges because the effective area curve there is affected by uncertainties in the model of the detector contaminant. Data were excluded in the following photon energy intervals: 0.52–0.55 (oxygen K edge), 0.68–0.73 (iron L edge) and 0.84–0.89 keV (neon K edge). Orders were combined through `add_grating_orders`. Despite the high count rates during the burst, none of the *Chandra* data are significantly piled up, due to the small frame time and large dispersion. The burst spectra were also independently extracted and fit using `idl` and `isis`, confirming all spectral fit results.

RXTE/PCA spectra were extracted from event mode data using ftool `seextrct`, filtering out artificial “clock events”. The PCA spectral response was calculated with `pcarsp` version 11.7.1. We find that the background model for PCU1 underestimates the spectrum beyond 30 keV, where no source photons are expected, by about 25%. To optimize the statistical quality and employ as many photons as possible, we chose to exclude the bandpass beyond 20 keV rather than to exclude PCU1 data. Below 20 keV the source photon spectrum is at least four times brighter than the background spectrum, so that the error is at most 3% (at 20 keV) for the non-burst emission and less for the burst emission. We verified the results with those obtained after excluding PCU1 and do not find significantly different results. Thus, we employ data of both active PCUs. The dead time fraction was calculated from standard-1 data following the prescription at the RXTE web site[6] and was found to be up to 23.3% at burst peak. This fraction was taken into account when calculating energy fluxes. All spectral bins up to 20 keV contained enough photons for Gaussian statistics to apply.

4. Spectral analysis

XSPEC version 12.7.1b was employed as analysis tool. *Chandra* and RXTE burst spectra were simultaneously modeled when investigating the continuum. RXTE data were fitted between 3 and 20 keV and *Chandra* data between 0.5 and 6 keV. All spectral bins were grouped so that each bin contains at least 15 photons. No background was subtracted from the *Chandra* spectra, while the particle-induced plus cosmic diffuse background was subtracted from the RXTE spectra (employing `pcabackest`). The *Chandra* background is expected to be a minor part (a few c s^{-1}, see *Chandra* website[7]) of the non-burst emission (117 c s^{-1} on average). We kept the normalization factor of the *Chandra* data with respect to the RXTE data to 1. When left free, the fit procedure finds a minimum χ^2_ν at a different normalization for every spectrum by adjusting other spectral parameters. Furthermore, the improvement in χ^2_ν is never more than about 1%. We conclude that the normalization is ill constrained. Thus, fluxes are calibrated against the PCA response.

Table 1. Spectral parameters of fit to non-burst or persistent *Chandra*/RXTE spectrum in 2.5 ks prior to burst.

Parameter	Fitted value
$N_{\rm H}$	$(0.88 \pm 0.04) \times 10^{21}$ cm^{-2}
Disk black body $kT_{\rm in}$	0.591 ± 0.006 keV
Disk black body $R^2_{\rm in}/D^2_{10\ \rm kpc}$	$(6.5 \pm 0.3) \times 10^2$ km^2
Power law photon index	1.892 ± 0.013
Power law flux at 1 keV	0.399 ± 0.014 ph s^{-1} cm^{-2} keV^{-1}
Gauss centroid	5.12 ± 0.09 keV
Gauss sigma	1.66 ± 0.06 keV
Gauss normalization	0.0156 ± 0.0012 phot s^{-1} cm^{-2}
χ^2_ν/ν	0.803/1530
0.5–20 keV flux	$(3.738 \pm 0.008) \times 10^{-9}$ erg cm^{-2} s^{-1}
0.5–60 keV abs. flux	4.772×10^{-9} erg cm^{-2} s^{-1}
0.5–60 keV unabs. flux	5.196×10^{-9} erg cm^{-2} s^{-1}

4.1. Chandra/RXTE pre-burst spectrum

A good representative of the non-burst emission during the burst may be obtained from data during the 2.5 ks prior to the burst. The flux remains approximately constant during that time and is similar to the flux immediately after the burst (for a high-quality light curve from RXTE data, see Fig. 3). Furthermore, there is simultaneous *Chandra* and RXTE data for this interval. We derived a satisfactory empirical model for these data consisting of a disk black body (e.g., Mitsuda et al. 1984), a power law and a Gaussian component, all absorbed by a single medium modeled according to the prescription in Wilms et al. (2000). The Gaussian component only applies to PCA data. It was also often needed in PCA spectra of other X-ray bursts (Galloway et al. 2008) and may be related to the collection of additional Galactic emission in the wide field of view of the PCA. Table 1 presents the best-fit model parameters. The value for $N_{\rm H}$ is within the range of values found previously by, for instance, Cackett et al. (2009) and Papitto et al. (2009).

4.2. Burst spectrum

We first fitted the burst data with an absorbed black body model, keeping the non-burst model fixed. This is the most common model applied to X-ray burst spectra. This model does not provide a statistically acceptable fit to the data for the first 20 s of the burst, neither the combined data nor the *Chandra* and RXTE data alone. This is illustrated in Fig. 4 (top panel) which shows the data for 2 to 5 s after burst onset when the temperature is varying by no more than 10% (see below), along with the best-fit model; the goodness of fit is $\chi^2_\nu = 3.58$ with $\nu = 267$ degrees of freedom. There is a strong excess at low photon energies, particularly in the *Chandra* data. In fact, the *Chandra* data alone are best fitted with a power law instead of a Planck function, in contrast to the RXTE data.

In order to find an explanation for the soft excess, we tested four spectral models. We did this in two time intervals, because the model needs to be applicable over all times. We chose time intervals 2–5 and 12–16 s, since during these times the spectrum does not vary much while the statistical quality is good. The first two models take into account inelastic scattering of photons by

---

[5] http://cxc.harvard.edu

[6] http://heasarc.gsfc.nasa.gov/docs/xte/recipes/pca_deadtime.html

[7] http://cxc.harvard.edu/contrib/maxim/bg/index.html

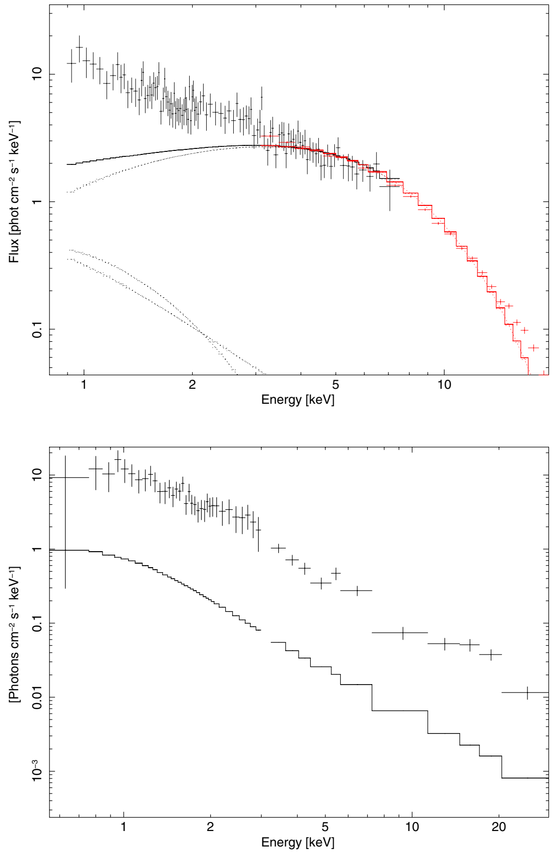

Fig. 4. Deconvolved spectra for 2 to 5 s after burst onset. The *top panel* shows the *Chandra* (black) and RXTE (red) spectrum. Data points are indicated by crosses and the total model by the histogram. The upper dotted curve represents the black body component and the lower two curved lines comprise the model components for the pre-burst radiation. The model is a bad fit ($\chi^2_\nu = 3.505$ for $\nu = 268$), but can be made consistent with the data by leaving free the normalization f_a of the non-burst model ($\chi^2_\nu = 0.963$ for $\nu = 267$). In the bottom panel the residual spectrum is plotted after subtraction of the fitted black body model (crosses). The model for the non-burst spectrum is plotted as a histogram. For clarity *Chandra* data is plotted up to 3 keV and RXTE data beyond 3 keV (only PCU2 to extend the energy range from 20 to 30 keV for visualization purposes). (Color version of figure available in online version.)

electrons in either the NS atmosphere or the accretion disk. The former was first put forward by London et al. (1986), further developed by Madej et al. (2004) and most recently calculated by Suleimanov et al. (2011, 2012). Hot atmospheric electrons harden the photons coming from below and increase the observed temperature to a value that is one to two times larger than the effective temperature. A soft excess remains (see Fig. 7 in Suleimanov et al. 2011). The model's free parameters are the luminosity in terms of the Eddington value and the NS radius. The fit of this model to the first data set (see Table 2) is insufficient, but that may be expected because model does not formally apply to radiation at the Eddington limit. The fit to the second data set, at sub Edddington flux levels, is not acceptable either. The data have a broader spectrum than the model.

Scattering by the accretion disk is calculated through the reflection model by Ballantyne (2004). In this model, black body radiation is assumed to hit the accretion disk and instantly photo-ionize it. The disk is modeled as a constant-density 1-dimensional slab. The radiation then is reprocessed by the disk and re-emitted into the line of sight. Above a few keV the reflected spectrum is very similar to the black body spectrum. Below a few keV it shows a soft excess whose detail depends on the level of ionization. The magnitude of the soft excess is a strong function of the density of the disk (see Fig. 4 in Ballantyne 2004). The total amount of reflection depends on the observer's viewing angle of the accretion disk. The model's free parameters are the black body temperature kT, the ionization parameter $\log \xi$ (ξ in units of erg cm s^{-1}) and the reflection fraction R. We first tested the disk model with density $n_\mathrm{H} = 10^{15}$ H-atoms cm^{-3} on the 2–5 s data, but this turns out to be unacceptable. A model with $n_\mathrm{H} = 10^{20}$ H-atoms cm^{-3} performs better and is able to fit the soft excess reasonably. The results are provided in Table 2. The reflection fraction turns out to be very large (10) for the 2–5 s data. It cannot be forced to smaller values by leaving free other parameters such as N_H. That may suggest that n_H is even higher, although 10^{23} cm^{-3} is close to the maximum value in standard accretion disk theory (Shakura & Sunyaev 1973). The strong coupling between R and n_H makes it difficult to obtain a good constraint on both, though. Unfortunately, due to increasing importance of 3-body interactions, there is no model yet available for higher n_H values.

The third model involves the addition of a second black body component with a different temperature. This is based on the possibility that there is exists a boundary layer between the accretion disk and the neutron star where radiation is released due to friction between both (Inogamov & Sunyaev 1999, 2010). Fits with this model are fairly good, see Table 2. We checked whether the small residual soft excess for the 2–5 s data is resolvable with a smaller value for N_H but it is not completely ($\chi^2_\nu = 1.229$ with $\nu = 266$ for $N_\mathrm{H} = 0$ cm^{-2}).

The fourth model is a straightforward variation of the initial model, namely to leave free the normalization f_a (with respect to the pre-burst value) of the persistent emission component listed in Table 1. This simple model was recently employed by Worpel et al. (2012) to model successfully 332 PCA-detected X-ray bursts with photospheric expansion in the 3–20 keV band. This model performs at least as well in terms of χ^2_ν as the double black body and reflection model, see Table 2, but on top of that it shows the least amount of systematic trend in the residuals for both spectra. Therefore, we chose to perform the full time-resolved spectral analysis with this model and note that the results for the primary black body component are similar as in the double black body model. Henceforth, we will call this the "f_a" model.

The "f_a" model is illustrated in the bottom panel of Fig. 4 where the 2–5 s spectrum is shown after the fitted black body model is subtracted. The model of the pre-burst spectrum is also shown. Over the 0.5–30 keV range shown, the shape is the same to a fairly accurate degree. To obtain a sense of how similar the persistent spectrum during this interval is to that before the burst, we left free in addition the power law and disk black body parameters. The best-fit power law index becomes 1.83 ± 0.05 and the disk black body $kT_\mathrm{in} = 1.23 \pm 0.64$ ($\chi^2_\nu = 0.701$ for $\nu = 263$). Therefore, it is somewhat harder.

We defined time bins covering 200 s from the burst onset, that were sufficiently short to resolve the spectral variations, while maintaining adequate signal-to-noise for precise spectral parameters. The adopted binning, achieved via trial-and-error, totaled 47 approximately logarithmically-spaced bins between 0.1 s at burst onset and 16 s in the tail. All time bins except one bridge the RXTE data gaps due to the full data buffer (see Sect. 2). In Fig. 5 we show the results of fitting the "f_a" model. The fits are excellent, except perhaps between 10 and 20 s, see Sect. 4.3. The soft excess remains until 20–30 s after the burst

Table 2. Fit results when attempting four different models (columns) to account for the soft excess on 2 data sets (rows).

NS atmosphere model	Reflection model	Double black body	“f_a” model
Time interval: 2–5 s (χ^2_ν = 3.505 with ν = 268 for black body fit)			
$\chi^2_\nu = 2.965$ ($\nu = 268$) $L/L_{\rm Edd} = 0.501 \pm 0.004$ $R = 16.49 \pm 0.09$ km	$\chi^2_\nu = 1.099$ ($\nu = 266$) $\log \xi = 3.60 \pm 0.03$ $kT = 2.27 \pm 0.03$ $R = 10.0 \pm 12.8$ ($n_{\rm H} = 10^{20}$ cm^{-3})	$\chi^2_\nu = 1.274$ ($\nu = 266$) $kT_1 = 0.620 \pm 0.017$ $F_1 = 18\%$ $kT_2 = 2.082 \pm 0.013$ $F_2 = 82\%$	$\chi^2_\nu = 0.963$ ($\nu = 267$) $kT = 1.985 \pm 0.009$ $F_{\rm bb} = 63\%$ $f_{\rm a} = 16.6 \pm 0.6$ $F_{f_{\rm a}} = 37\%$
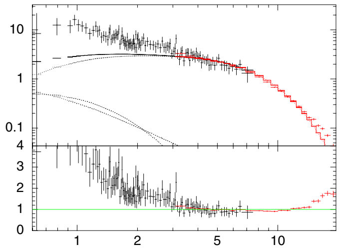	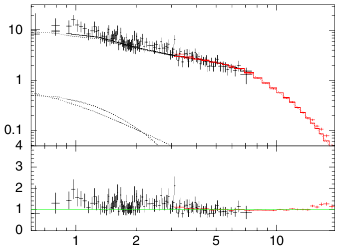	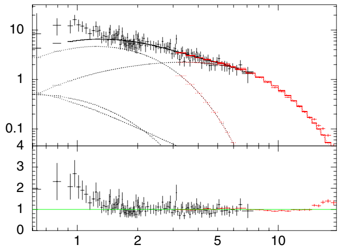	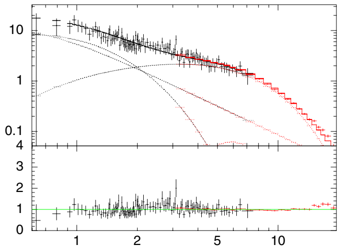
Time interval: 12–16 s (χ^2_ν = 1.792 with ν = 148 for black body fit)			
$\chi^2_\nu = 1.893$ ($\nu = 148$) $L/L_{\rm Edd} = 0.293 \pm 0.002$ $R = 13.76 \pm 0.08$ km	$\chi^2_\nu = 0.954$ ($\nu = 146$) $\log \xi = 3.61 \pm 0.14$ $kT = 1.84 \pm 0.02$ $R = 0.38 \pm 0.24$ ($n_{\rm H} = 10^{20}$ cm^{-3})	$\chi^2_\nu = 0.693$ ($\nu = 146$) $kT_1 = 1.593 \pm 0.046$ $F_1 = 73\%$ $kT_2 = 2.82 \pm 0.34$ $F_2 = 27\%$	$\chi^2_\nu = 1.341$ ($\nu = 147$) $kT = 1.790 \pm 0.007$ $F_{\rm bb} = 80\%$ $f_{\rm a} = 3.7 \pm 0.3$ $F_{f_{\rm a}} = 20\%$
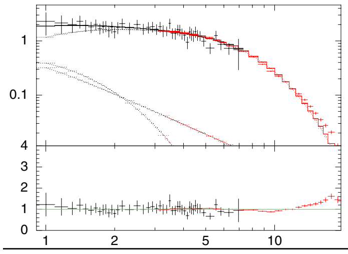	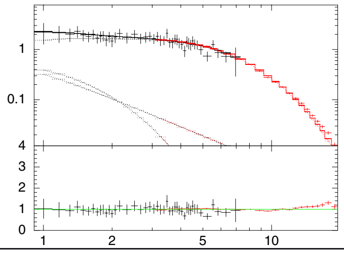	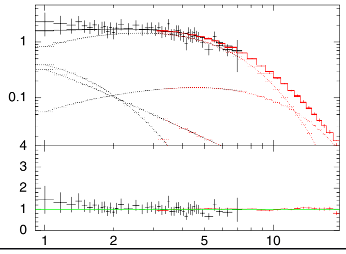	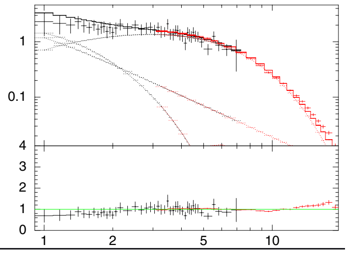

Notes. First order LETGS spectra were combined and binned to 15 photons per bin. The figures show the deconvolved spectra (top panels; in units of phot cm^{-2} s^{-1} keV^{-1}) and their relative deviation (i.e., data divided by the predicted model value; bottom panels) with respect to the models. Black curves are for LETGS and red for RXTE data. The y-axes for the bottom panels have identical scales. (Color version of table available in online version.)

onset. In Fig. 6 we plot $f_a - 1$ against the burst bolometric flux. This shows that the increase of the persistent spectrum is present for burst fluxes above 10% of the peak flux and that its flux is not a simple constant fraction of the thermonuclear burst flux.

The peak radius reached during the expansion interval was 10 km, a factor of approximately 2 larger than the radius at touchdown. This degree of expansion is quite modest; in the strongest radius expansion bursts, the radius expands to at least 10^2 times the NS radius. We note that, similar to other bursts from this source, the radius increases following touchdown up to a level comparable to the maximum reached during the expansion. However, this increase during the burst tail is usually attributed to a decrease in the spectral correction factor as the flux decreases (e.g., Suleimanov et al. 2011) so that the photospheric radius during the expansion is significantly in excess of the NS radius.

The burst reaches a peak flux of $(2.50 \pm 0.16) \times 10^{-7}$ erg cm^{-2} s^{-1} (after accounting for the increased persistent emission), and the bolometric burst fluence is $f_{\rm burst} = (3.41 \pm 0.04) \times 10^{-6}$ erg cm^{-2} over 184 s. Table 3 presents the complete set of derived burst parameters. One can estimate the burst recurrence time according to $t_{\rm recur} = \alpha \times f_{\rm burst}/F_{\rm pers}$, where $\alpha \approx 150$ (Galloway & Cumming 2006) and bolometric persistent flux $F_{\rm pers} = 6 \times 10^{-9}$ erg cm^{-2} s^{-1}. This results in $t_{\rm recur} \approx 80$ ks. This is similar to the maximum continuous data set available around the burst (see Fig. 2). An interesting number is the total number of bursts expected in the whole outburst. If we assume a Crab spectrum for the whole outburst, the total fluence under the estimated integral of the outburst light curve (Fig. 2) would be about $f_{\rm outburst} = 2.9 \times 10^{-3}$ erg cm^{-2}. The total number of expected bursts would then be $f_{\rm outburst}/\alpha f_{\rm burst} \approx 6$. The net coverage of the RXTE and *Chandra* observations is only 2.5 d compared to roughly 25 d for the whole outburst. Thus, it is not unexpected to have detected only one burst.

4.3. Search for absorption edges

We extracted full-resolution orders −1 and +1 of the LETGS data for the first 20 s and fitted the spectrum after subtraction of the pre-burst spectrum with a power law and show in Fig. 7 the deviations of the data with respect to the continuum model. The goodness of fit is $\chi^2_\nu = 0.684$ ($\nu = 678$). There is no obvious sought-after edge visible. We determined the 90% confidence

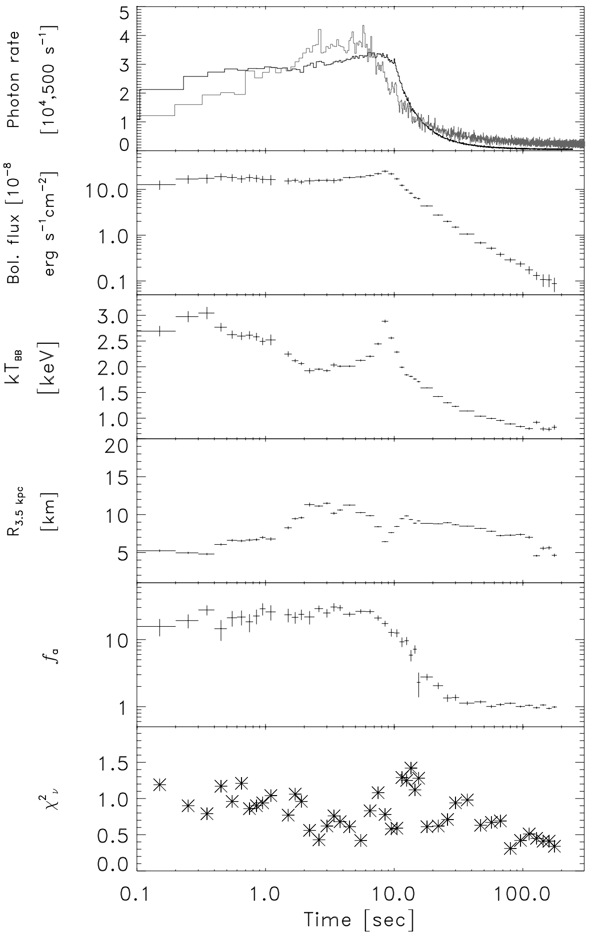

Fig. 5. Time-resolved spectral analysis results for the combined RXTE/*Chandra* data sets. The *top panel* shows the photon count rates in both instruments: gray for *Chandra*-LETGS (in units of 500 s^{-1}) and black for RXTE-PCA (in units of 10^4 s^{-1}).

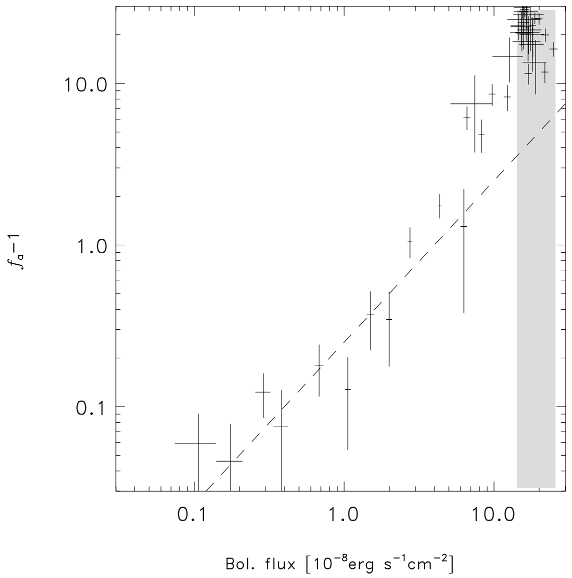

Fig. 6. Persistent emission flux pre-factor f_a minus 1 versus bolometric burst flux measurements (see also Fig. 5). The gray area indicates the region of the Eddington limit, between that for a hydrogen and a helium photosphere. The dashed line shows how the trend should go if the flux ratio of the increased persistent spectrum to burst would be constant.

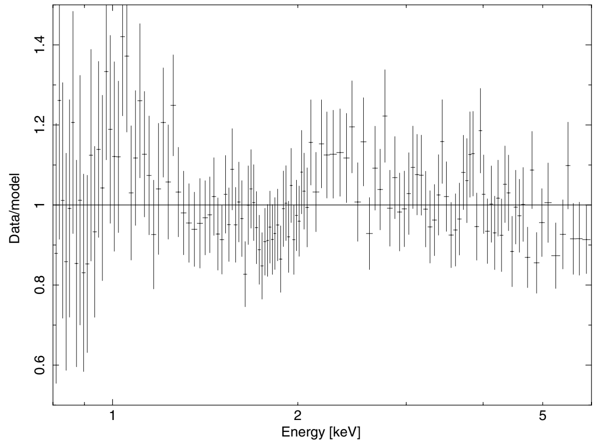

Fig. 7. Combined and rebinned first-order LETGS spectrum of data from the first 20 s of the bursts, in terms of fractional residuals with respect to an empirical continuum fit.

upper limits on the equivalent width[8] of any absorption edge by fixing a model for the edge at various photon energies, leaving free the power law parameters and edge depth while fixing N_H and determining the edge depths for which χ^2 is 2.7 above the minimum value. We find the upper limit to range between 20 eV at 1.8–2.4 keV to 200 eV at 1.3 and 3.3 keV up to 400 eV at 5.0 keV, see Fig. 8.

There is a broad dip at 1.8 keV which may arise from a broad absorption line or edge feature. Fitting it with an absorption line yields a centroid energy of 1.77 ± 0.04 keV, a line width of $\sigma = 0.15 \pm 0.05$ keV and an equivalent width of -56 ± 15 eV. The goodness of fit is $\chi^2_\nu = 0.624$ ($\nu = 673$). Fitting it with an absorption edge yields an edge energy of 1.29 ± 0.01 keV and an optical depth of 0.29 ± 0.06 with $\chi^2_\nu = 0.648$ ($\nu = 676$). Adding a second edge does not really improve the fit, with $\chi^2_\nu = 0.641$ ($\nu = 674$).

We searched for edges in smaller time frames and found none. The upper limits are a factor of 4 to 5 worse at 1 s resolution than at 20 s.

In the RXTE data we analyzed the spectra with the highest χ^2_ν values: between 6 and 8 s (this is near the touch-down point) and between 12 and 16 s. These spectra show spectral deviations which are reminiscent of the shape of an absorption edge with an energy between 7 and 8 keV and an optical depth of 0.2–0.3 (equivalent width 0.7–1.1 keV). Unfortunately, these edges are not covered by the *Chandra* data so we cannot get confirmation from there. We repeated the time-resolved spectroscopic analysis illustrated in Fig. 5, but adding an absorption edge and find that the data are consistent with the continuous presence of the above mentioned edge, but that it is detectable only when the statistical quality of the data are sufficient to allow detection which is between roughly 6 and 40 s after burst onset.

4.4. Search for spectral lines

We searched for absorption and emission lines in the LETGS data during five time intervals: 0–2 s during the burst rise, 2–5 s during the first part of the peak, 5–9 s during the second part of the peak, 9–12 s during the first part of the tail and 12–16 s

---

[8] We define the equivalent width as the integral over energy E of $1 - \exp\left(-\tau\left(\frac{E}{E_0}\right)^3\right)$ with E_0 the edge energy and τ its optical depth.

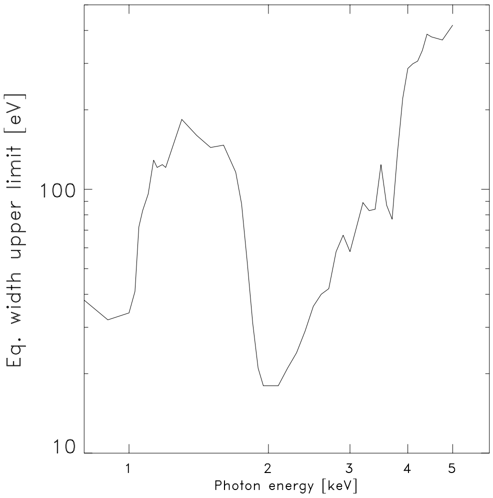

Fig. 8. For the 20 s exposure (see Fig. 7), this graph shows the upper limits of an absorption edge as a function of photon energy.

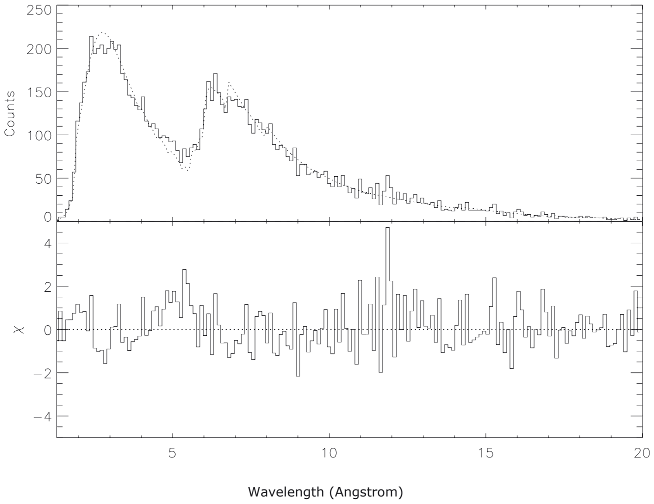

Fig. 9. *Chandra*-LETGS burst spectrum between 0 and 7 s after burst onset, in wavelength domain. The histogram represents the data and the dotted line a continuum fit. *Top panel* is the spectrum, *bottom panel* the deviation with respect to the fitted model in units of σ. Note the feature at 11.9 Å.

during the second part of the tail. A 4.0σ detection threshold was employed. This is equivalent to one chance detection in all 20 000 trials. The number of trials is determined as follows: 200 independent tests per 2–12 Å spectrum with a LETGS resolution and binning of 0.05 Å; a factor of 2 for five successive 2 times binned-up versions of the spectra; and a factor of 5 for the five time intervals mentioned above. In order to have a 10% chance of a false positive (in either absorption or emission), a one-tailed test would require a 1 in 20 000 chance for detection in random data, which is about 4.0 sigma. We also searched in 4 different time intervals (0–7, 2–4, 4–6, and 7–30.5 s) that overlap the above time intervals.

The strongest candidate line that we find is an emission feature that we find in the 0–7 s time interval at 11.9 Å (or 1.04 keV), see Fig. 9. This feature is 4.7σ above the continuum in a binning of 0.11 Å. Given that we searched in additional time intervals, the significance should be diminished to 4.6σ. The equivalent width is about 4 Å.

5. Timing analysis

We performed a timing analysis of the RXTE data of the burst, by generating Fourier power spectra for 10-s data stretches every 1 s, employing the event mode data with 125 μs resolution. We limited the analysis to channels 5–37 (2–10 keV), where the ratio of the burst photon rate to the background rate is highest. We detect burst oscillations with a burst fractional amplitude of 2–5% rms in the tail. This value is calculated without taking into account the contribution of the accretion powered pulsations that might still be present at the time of the burst. This correction is relatively small since the accretion powered pulsations have pulsed fractions of 3–4% rms prior and after the occurrence of the burst (see for example Patruno et al. 2012). Furthermore the photon count rate detected when burst oscillations are seen is between two and four times the count rate received prior to the occurrence of the burst, meaning that the oscillations seen are truly of nuclear origin (see e.g., Eq. (11) in Watts et al. 2005). Similar considerations apply to the burst oscillation phase, which are negligibly influenced by the presence of accretion powered pulses. Burst oscillations were marginally detected (between 2 and 3 sigma for 1 s long trains) at 400–401 Hz during the burst rise with fractional rms amplitudes of up to 5%.

The formal 90%-confidence upper limit on the fractional rms amplitude is 8%. This is consistent with measurements of previous bursts from SAX J1808.4−3658 with RXTE (Chakrabarty et al. 2003; Bhattacharyya & Strohmayer 2006) where amplitudes were seen between 5 and 25% in 0.25 s long trains. Our data is less sensitive because of the smaller number of active PCUs (2 instead of 4).

The time resolution of the ACIS-S CC mode data is 2.85 ms (351 Hz). This implies that the burst oscillation signal (401 Hz) cannot be easily resolved in the *Chandra* data. Simulations show that to detect a sinusoidal pulsation at 401 Hz in a 1 s stretch of data with a resolution of 2.85 ms requires a relative rms amplitude of at least 25% to be significantly detected as an alias at 401–351 = 50 Hz which is an order magnitude larger than ever detected for SAX J1808.4−3658.

6. Discussion

The 2011 outburst of SAX J1808.4−3658 is the seventh since its discovery in 1996 (in 't Zand et al. 1998), and comes 3 years after the previous outburst. Galloway (2008) found that the onset time of the earlier outbursts followed a quadratic relation with time, which predicted the time of the previous outburst to within 11 d. However, the 2011 outburst occurred 197 d earlier than predicted, suggesting that the long-term mass transfer rate may be increasing. We estimated the total fluence for the outburst as ≈2.9×10^{-3} erg cm^{-2}, which is significantly lower than for the first four outbursts (Galloway 2006). Thus, it seems likely that the long-term accretion rate remains substantially below that of the first decade of observations.

6.1. Peak flux and burst oscillations

The thermonuclear burst detected from SAX J1808.4−3658 on 2011 November 8 is the brightest ever detected with *Chandra*, and the second brightest with RXTE. Within the 1907 ks exposure time on SAX J1808.4−3658 during the complete RXTE mission, this is the ninth burst (e.g., Galloway et al. 2008). The second brightest burst has a peak flux of $(2.40 \pm 0.03) \times 10^{-7}$ erg cm^{-2} s^{-1} (this is burst No. 4 in Galloway et al. 2008,

Table 3. Burst parameter values, extracted from RXTE data alone for easy comparison with other bursts (e.g., Galloway et al. 2008).

Parameter	Value
Onset time	MJD 55 873.91320 (barycentered) 2011 Nov. 8 21:55:00.50 UTC 563 407 175.90 s RXTE MET 437 176 836.46 s *Chandra* MET
Rise times	2.5 ± 0.1 s (25 to 90% of peak) 6.3 ± 0.1 s (0 to 100%) 0.1 ± 0.1 s (0 to 70%)
e-folding decay time	12.0 s
Time scale (fluence/peak flux)	12.9 s
Duration	≈500 s (down to 0.03% of peak flux)
Unabs. bol. peak flux	$(2.56 \pm 0.15) \times 10^{-7}$ erg cm^{-2} s^{-1}
Unabs. bol. fluence	$(3.41 \pm 0.04) \times 10^{-6}$ erg cm^{-2}
3–20 keV persistent flux	1.72×10^{-9} erg cm^{-2} s^{-1}
0.5–60 keV unabsorbed flux	6.1×10^{-9} erg cm^{-2} s^{-1}

Notes. Times are not barycentered.

note that this publication lists peak fluxes before dead time correction) that is only slightly fainter than the brightest. Our burst is otherwise fairly ordinary for SAX J1808.4−3658, including its timing behavior. Galloway & Cumming (2006) find that bursts from SAX J1808.4−3658 are due to flashes in a hydrogen-depleted layer and burn primarily helium.

The Eddington limit of a solar-composition photosphere on the surface of a 10 km radius NS of mass 1.4 $M_\odot$ at a distance of 3.5 kpc corresponds to a flux of 1.4×10^{-7} erg cm^{-2} s^{-1}, for a helium-rich photosphere 2.6×10^{-7} erg cm^{-2} s^{-1}. The peak flux for the burst from SAX J1808.4−3658 is within this range, clearly indicating that the energy production rate due to the thermonuclear flash is consistent with the Eddington rate. It is perhaps worth noting here that the distance estimate of 3.5 kpc for SAX J1808.4−3658 comes from a comparison of the measured burst energetics and recurrence times with the predictions of theoretical ignition models (Galloway & Cumming 2006), not merely from the peak flux of previous PRE bursts, as is the case for the majority of LMXB distances. While the time dependence of the black body temperature and normalization is also characteristic for an Eddington-limited burst, with the typical "touchdown" peak at 10 s (see Fig. 5), the radius expansion is limited to at most a factor of about 2. This is typical for moderate expansion (in 't Zand & Weinberg 2010). There is no evidence for the expulsion of a shell, such as a (short) precursor. Ergo, this is not a superexpansion burst (see Sect. 1).

The accretion flux prior to the burst translates to a 0.5–20 keV luminosity of 4.5×10^{36} erg s^{-1} for a distance of 3.5 kpc, or 64 times smaller than the burst peak in the same bandpass.

The burst oscillations detected in this burst are very similar to those detected in the RXTE data of previous bursts. The amplitude compares well with the fractional rms amplitude of 2–4% in previous bursts (Watts 2012; Patruno & Watts 2012).

6.2. Broad-band spectrum

The *Chandra* data are interesting for the peculiar behavior of the burst spectral continuum. As illustrated in Fig. 4, data below 3–4 keV draw a rather different picture of the burst spectrum than above. The sub-3 keV data reveal a strong soft excess above the black body. This is not the first time that a soft excess is observed in a burst spectrum, although it seems to be a rare phenomenon, possibly because many bursters have too much interstellar absorption to allow detection of a soft excess. We count about 250 X-ray bursts that have been detected with sub 3 keV coverage by *XMM-Newton*, *Chandra* and *Swift*-XRT (e.g., Kong et al. 2007; in 't Zand et al. 2009; Galloway et al. 2010). Most of these do not show photospheric expansion. Only Asai & Dotani (2006) and Boirin et al. (2007) report on strong soft excesses found in some bursts from the eclipsing LMXB EXO 0748−676. They propose that this is due to a decrease in absorption by the circumstellar medium arising from the photoionization of that medium by the burst photons, thereby allowing more accretion disk flux to reach the X-ray detector. This explanation may be plausible for a high-inclination system (i = 75°–83° for EXO 0748−676; Parmar et al. 1986), but for SAX J1808.4−3658 the inclination angle is suggested to be low (<67°; Deloye et al. 2008), so there is little local obscuring material affecting the spectrum. We note that the two published *Chandra* HETGS grating observations of 33 X-ray bursts (including 4 with photospheric expansion; Thompson et al. 2005; Galloway et al. 2010) could have found soft excesses of similar magnitude as in SAX J1808.4−3658, had they been present.

The net burst spectrum is not consistent with the NS atmosphere model of Suleimanov et al. (2011). There is better agreement with the model for reflection against the accretion disk and even better with the simple double black body model. Mildly better overall is the agreement with the "f_a" model, because this models appears to have the smallest systematic trends in its residuals (see bottom panels of figures in Table 2). In a study of 332 radius-expansion bursts seen with RXTE, Worpel et al. (2012) modeled the 3–20 keV spectra in the same "f_a" manner. They found as a general feature that f_a is significantly in excess of 1, with the highest values arising from the bursts observed at the lowest pre-burst fluxes. Our combined *Chandra*-RXTE analysis of one burst from SAX J1808.4−3658 is consistent with those results and shows additionally that this behavior extends to lower energies, giving rise to a large flux excess below 3 keV for a system with low N_H (see Fig. 4). However, we note that the difference in performance with other models is not much better. It is in the spirit of Occam's Razor (with only 1 additional free parameter) that we provide the full time-resolved spectroscopic analysis in terms of the simple "f_a" model, but other models are almost equally justified.

Worpel et al. (2012) suggest that the increase of the non-burst emission is caused by the Poynting-Robertson (PR) effect, which removes angular momentum from the inner accretion disk due to radiation drag, thereby increasing the accretion rate during the burst. If the accretion rate in SAX J1808.4−3658 increased by a factor of 20 during the burst, based on our maximum best-fit value of f_a, it would come close to 50% of the Eddington limit. Significant changes in the persistent spectral state might be expected, analogous to the so-called spectral state changes of the persistent emission that are attributed to changes in the geometry of the accretion disk (e.g., Done et al. 2007, and references therein). Since the persistent spectrum of SAX J1808.4−3658 at the time of the burst is quite hard, a softening of the spectrum seems most likely. However, it is not obvious that a typical hard-to-soft spectral state change can take place in response to an increase in accretion rate sustained for ≲20 s, or even if the effects of PR drag would produce the same observable effect. Our data suggests that, if there is a change, the persistent spectrum instead becomes harder during the burst.

We note also that if the accretion rate increases by a factor of 20 over 10 s, the additional matter must be that which would otherwise have been accreted over the next 200 s, and one would thus expect a suppression of the accretion rate following the burst. This would be the hallmark of the PR effect taking place. We found no evidence of f_a values smaller than 1, out to 500 s after the burst. However, the recuperation time of the disk may be longer if the disk viscosity is relatively small (Walker 1992), so that the suppressed accretion rate would be spread out over a longer interval, and hence undetectable.

The pre-burst spectrum likely includes a component from inverse Compton scattering of undetectable soft photons (with energies <0.5 keV for this burst) by an accretion disk corona (ADC; White & Holt 1982; Begelman et al. 1983; Begelman & McKee 1983). An increase in the persistent spectrum would therefore require either a larger ADC, or an increase of soft seed photons into the ADC. The burst cannot produce a larger ADC through photoionization, as the temperature of the plasma can only be raised to its Compton temperature which is $\approx kT$ for a blackbody spectrum. This temperature is much lower than the >10 keV temperature required to explain the high-energy extent of the persistent emission. Likewise, since the local dissipation in the accretion disk scales as R^{-3} (where R is the radius along the disk), expansion of the ADC outwards through a wind or outflow would not be able to explain the significant increase in the ADC emission. This constraint could be circumvented if the disk and ADC were expanded inwards by the burst, as through Poynting-Roberston drag (see discussion above).

Perhaps the simplest explanation for an increase in the persistent spectrum during the burst is a larger influx of seed photons produced by reprocessing in the accretion disk. As discussed in Sect. 4.2, high density reflection models were able to explain a large fraction of the strong soft excess seen early on in the burst. This emission, which extends below 0.5 keV, is dominated by thermal bremsstrahlung produced by the X-ray heated outer layers of the disk (Ballantyne 2004; Ballantyne & Everett 2005), and is a natural source of additional seed photons to the corona. This explanation has several advantages: first, the absorption and re-emission of the burst will all occur on not much more than twice the light-crossing time of the system, and would explain why the enhanced persistent emission is seen even in the earliest phases of the burst. Similarly, Figs. 5 and 6 illustrate that the increase in the persistent flux falls rapidly as the illuminating blackbody fades, which would be a natural consequence of less reprocessing in the inner disk. Finally, if reprocessing accounts for most of the soft excess, then this reduces the values of f_a required to fit the spectra. Nevertheless, this idea remains just informed speculation, and further study of the broadband spectra of Type 1 X-ray bursts, as well as a concentrated theoretical effort into understanding the interaction of a burst with the surrounding accretion flow, is needed to understand the physical processes at work in these environments.

6.3. Evidence for spectral features

The high spectral resolution data provided by the *Chandra*/LETGS show no evidence for the sought-after absorption edge with upper limits in the equivalent width of at best 20 eV. The residuals between 1 and 2 keV with respect to a continuum fit (Fig. 7) are not clearly identifiable with a single absorption edge or two. A single edge would have an energy of 1.29 keV. For a gravitational redshift anywhere between $1 + z = 1$ for far away from the NS and $1 + z = 1.31$ on the surface (for a NS with mass 1.4 $M_\odot$ and radius 10 km), the expected range of edge energies is 1.3–1.8 keV. This is not identifiable with a K or L-edge of any likely element. The redshifted K-edge of hydrogen-like Si comes closest at 2.0 keV. Only K-edge energies of Mg and Al and L-edge energies of Ga, Ge, As, Se and Br would fit. Also, the residuals in this energy range are likely to be affected by a sharp change in the effective area arising from the K-edge of the neutral silicon CCD material.

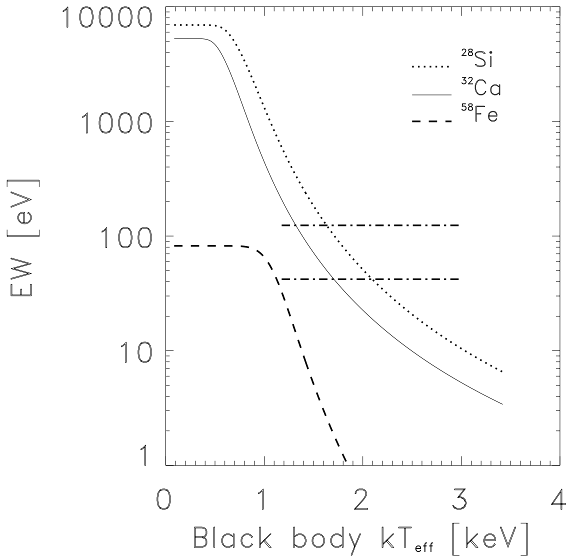

Fig. 10. For the 20 s exposure (see Figs. 7 and 8), this graph shows the upper limits of an absorption edge at 2.67 keV (lower horizontal dash-dotted line) and 3.48 keV (upper horizontal line), compared to the predictions for the K-edge of hydrogen-like ^{28}Si (dotted curve), ^{32}Ca (solid curve) and ^{56}Fe (dashed curve), for abundances as determined from the He0.1 model (pure helium ignition at 0.1 $\dot{M}_{\rm Edd}$) in Weinberg et al. (2006). The range where the upper limits apply are set by the range of black body color temperatures measured (2–3 keV) multiplied with a maximum possible color correction of 0.6 to arrive at effective temperatures (e.g., Suleimanov et al. 2011). The upper limits would be 3 to 4 times better if the edge energy would be gravitationally redshifted by a factor of 1.31. They are 4.5 times worse for an exposure time of 1 s.

For a 20 s exposure, the upper limit on the equivalent width ranges between 42 eV at the Si K-edge (2.67 keV) and 124 eV at the Ca K-edge (3.48 keV). These are the two most abundant elements expected for pure helium ignition according to Weinberg et al. (2006) with the largest predicted absorption edges. These upper limits are compared with predicted values in Fig. 10. The predictions are for ignition in a pure helium layer like for SAX J1808.4−3658 (Galloway & Cumming 2006). The predictions are at (for Si) or below the measured upper limits. Thus, these measurements are consistent with predictions. We note that the tentative edge detected in the RXTE data at about 7.9 keV has an equivalent width of 0.7–1.1 keV and is, thus, much higher than the prediction for the Fe-K edge. On the other hand, the picture that this edge draws is not consistent with the expectation. The edge energy and optical depth are consistent with being constant while the temperature of the photo-ionizing radiation field changes between 3 and 1 keV. This is different from the features seen by in 't Zand & Weinberg (2010) and suggests one should be careful in associating this feature with matter close to the NS.

We find marginal evidence for an emission line at 11.9 Å with an equivalent width of 4 Å. This wavelength resides in the range of rest wavelengths of a number of Ne lines and is slightly blue-shifted from the Fe L line complex. We believe the line is too marginal to draw any further physical conclusions. However, it is interesting to note that recently a strong emission line has been detected (Degenaar et al. 2013) at about the same energy in a long superexpansion burst, with an equivalent width that is about 3 times smaller than the feature we see, but for a much longer duration (10 min).

Although this burst is Eddington limited, it does not exhibit strong photospheric expansion. Such expansion will probe the predictions at lower black body temperatures in Fig. 10. Thus, the sensitivity would be better. We suggest to focus future searches for absorption edges on burst with those, ergo the "superexpansion" bursts, since these have not yet been detected at high spectral resolution. The most opportune sources to search in are 4U 1820-30 (in globular cluster NGC 6624) and 4U 1724-30 (in globular cluster Terzan 2), because they show bursts every few hours to days (4U 1820-30 in the low/hard state) with at least 25% of the time superexpansion (in 't Zand & Weinberg 2010; in 't Zand et al. 2012).

7. Conclusion

A simultaneous *Chandra*-LETGS/RXTE detection of a very bright thermonuclear X-ray burst with moderate photospheric expansion and low $N_{\rm H}$ presents a unique opportunity to study the 0.5–30 keV spectrum of such an event, with large sensitivity and high spectral resolution below 6 keV. We find that

- The spectrum show a strong deviation from black body radiation, particularly at low energies where it exhibits a soft excess that exceeds the black body by an order of magnitude. The non-Planckian component has a similar spectral shape as the pre-burst spectrum that is powered by accretion, suggesting that the accretion flow changes during the burst, probably due to the near-Eddington flux from the burst. Exactly how that happens is difficult to determine, mostly because there is no detailed model yet available for the dynamic and radiative interaction of a burst with the pre-existing accretion flow, but most likely it is related to an increase of seed photons in the ADC. Future work should include a hydrodynamic model of the interaction between X-ray bursts and accretion disks and a comprehensive of study of f_a values over bursts with and without photospheric expansion;
- No unambiguous spectral features are detected. The upper limits for absorption edges are, however, consistent with the theoretically predicted equivalent widths due to ejected ashes. It is expected that edges are deeper for bursts with photospheric superexpansion. Therefore, future searches with *Chandra* should preferably concentrate on those. This is also underlined by the recent finding by Degenaar et al. (2013). Regarding absorption edges in bursts with moderate photospheric expansion, investigating superbursts with current grating spectrometers would be interesting and, in the farther future, the proposed LOFT mission with 10 m^2 of silicon drift detectors (Feroci et al. 2012) has the right combination of sensitivity and spectral resolution to make progress.

Acknowledgements. We thank Valery Suleimanov, Juri Poutanen, Tullio Bagnoli, Hauke Worpel, Daniel Haas, David Huenemoerder for useful discussions, and Suleimanov and Poutanen for making available their model in a form that is suitable for use in XSPEC. We are grateful to Harvey Tananbaum, Nancy Wolk, Jeremy Drake and the *Chandra* team for their support of this quick (3.5 d turn around) TOO. J.Z. and D.G. acknowledge ISSI for the hospitality in Bern where part of this work was performed. This research has made use of data and software, in the application package `ciao`, provided by the *Chandra* X-ray Center (CXC), RXTE data provided by the RXTE Guest Observer Facility, MAXI data provided by RIKEN, JAXA and the MAXI team, and *Swift*/BAT data provided by the *Swift*/BAT team.

References

Asai, K., & Dotani, T. 2006, PASJ, 58, 587
Ballantyne, D. R. 2004, MNRAS, 351, 57
Ballantyne, D. R., & Everett, J. E. 2005, ApJ, 626, 364
Barthelmy, S. D., Barbier, L. M., Cummings, J. R., et al. 2005, Space Sci. Rev., 120, 143
Begelman, M. C., & McKee, C. F. 1983, ApJ, 271, 89
Begelman, M. C., McKee, C. F., & Shields, G. A. 1983, ApJ, 271, 70
Bhattacharyya, S., & Strohmayer, T. E. 2006, ApJ, 642, L161
Boirin, L., Keek, L., Méndez, M., et al. 2007, A&A, 465, 559
Brinkman, A. C., Gunsing, C. J. T., Kaastra, J. S., et al. 2000, ApJ, 530, L111
Cackett, E. M., Altamirano, D., Patruno, A., et al. 2009, ApJ, 694, L21
Chakrabarty, D., Morgan, E. H., Muno, M. P., et al. 2003, Nature, 424, 42
Cottam, J., Paerels, F., & Mendez, M. 2002, Nature, 420, 51
Degenaar, N., Miller, J. M., Wijnands, R., Altamirano, D., & Fabian, A. C. 2013, ApJ, 767, L37
Deloye, C. J., Heinke, C. O., Taam, R. E., & Jonker, P. G. 2008, MNRAS, 391, 1619
Done, C., Gierliński, M., & Kubota, A. 2007, A&A Rev., 15, 1
Feroci, M., Stella, L., van der Klis, M., et al. 2012, Exp. Astron., 34, 415
Galloway, D. K. 2006, in The Transient Milky Way: A Perspective for MIRAX, eds. F. D'Amico, J. Braga, & R. E. Rothschild, AIP Conf. Ser., 840, 50
Galloway, D. 2008, in 40 Years of Pulsars: Millisecond Pulsars, Magnetars and More, eds. C. Bassa, Z. Wang, A. Cumming, & V. M. Kaspi, AIP Conf. Ser., 983, 510
Galloway, D. K., & Cumming, A. 2006, ApJ, 652, 559
Galloway, D. K., Muno, M. P., Hartman, J. M., Psaltis, D., & Chakrabarty, D. 2008, ApJS, 179, 360
Galloway, D. K., Yao, Y., Marshall, H., Misanovic, Z., & Weinberg, N. 2010, ApJ, 724, 417
Garmire, G. P., Bautz, M. W., Ford, P. G., Nousek, J. A., & Ricker, Jr., G. R. 2003, in SPIE, eds. J. E. Truemper, & H. D. Tananbaum, SPIE, Conf. Ser., 4851, 28
in 't Zand, J. J. M., & Weinberg, N. N. 2010, A&A, 520, A81
in 't Zand, J. J. M., Heise, J., Muller, J. M., et al. 1998, A&A, 331, L25
in 't Zand, J. J. M., Cornelisse, R., Kuulkers, E., et al. 2001, A&A, 372, 916
in 't Zand, J. J. M., Keek, L., Cumming, A., et al. 2009, A&A, 497, 469
in 't Zand, J. J. M., Homan, J., Keek, L., & Palmer, D. M. 2012, A&A, 547, A47
Inogamov, N. A., & Sunyaev, R. A. 1999, Astron. Lett., 25, 269
Inogamov, N. A., & Sunyaev, R. A. 2010, Astron. Lett., 36, 835
Jahoda, K., Markwardt, C. B., Radeva, Y., et al. 2006, ApJS, 163, 401
Jonker, P. G., Méndez, M., Nelemans, G., Wijnands, R., & van der Klis, M. 2003, MNRAS, 341, 823
Kong, A. K. H., Miller, J. M., Méndez, M., et al. 2007, ApJ, 670, L17
Lewin, W. H. G., van Paradijs, J., & Taam, R. E. 1993, Space Sci. Rev., 62, 223
London, R. A., Taam, R. E., & Howard, W. M. 1986, ApJ, 306, 170
Madej, J., Joss, P. C., & Różańska, A. 2004, ApJ, 602, 904
Markwardt, C. B., Palmer, D. M., Barthelmy, S. D., et al. 2011, The Astronomer's Telegram, 3733, 1
Matsuoka, M., Kawasaki, K., Ueno, S., et al. 2009, PASJ, 61, 999
Mitsuda, K., Inoue, H., Koyama, K., et al. 1984, PASJ, 36, 741
Paizis, A., Nowak, M. A., Rodriguez, J., et al. 2012, ApJ, 755, 52
Papitto, A., Di Salvo, T., D'Aì, A., et al. 2009, A&A, 493, L39
Parmar, A. N., White, N. E., Giommi, P., & Gottwald, M. 1986, ApJ, 308, 199
Patruno, A., & Watts, A. L. 2012 [`arXiv:1206.2727`]
Patruno, A., Bult, P., Gopakumar, A., et al. 2012, ApJ, 746, L27
Shakura, N. I., & Sunyaev, R. A. 1973, A&A, 24, 337
Strohmayer, T., & Bildsten, L. 2006, New views of thermonuclear bursts (Compact stellar X-ray sources), 113
Suleimanov, V., Poutanen, J., & Werner, K. 2011, A&A, 527, A139
Suleimanov, V., Poutanen, J., & Werner, K. 2012, A&A, 545, A120
Thompson, T. W. J., Rothschild, R. E., Tomsick, J. A., & Marshall, H. L. 2005, ApJ, 634, 1261
van Paradijs, J., Dotani, T., Tanaka, Y., & Tsuru, T. 1990, PASJ, 42, 633
Walker, M. A. 1992, ApJ, 385, 642
Wang, Z., Chakrabarty, D., Roche, P., et al. 2001, ApJ, 563, L61
Watts, A. L. 2012, ArXiv e-prints
Weinberg, N. N., Bildsten, L., & Schatz, H. 2006, ApJ, 639, 1018
White, N. E., & Holt, S. S. 1982, ApJ, 257, 318
Wijnands, R., & van der Klis, M. 1998, Nature, 394, 344
Wilms, J., Allen, A., & McCray, R. 2000, ApJ, 542, 914
Worpel, H., Galloway, D., & Price, D. 2012, ApJ, submitted [`arXiv:1303.4824`]